PERGAMON

International Journal of Solids and Structures 36 (1999) 5639–5661

INTERNATIONAL JOURNAL OF SOLIDS and STRUCTURES

www.elsevier.com/locate/ijsolstr

Elastic-plastic analysis of biaxially loaded center-cracked plates

N.P. O'Dowd[a,*], O. Kolednik[b], V.P. Naumenko[c]

[a] *Department of Mechanical Engineering, Imperial College, Exhibition Road, London SW7 2BX U.K.*

[b] *Erich Schmid Institut für Festköperphysik der Österreichischen Akademie der Wissenschaften, Jahnstr. 12 A-8700 Leoben, Austria*

[c] *Institute for Problems of Strength, National Academy of Sciences of the Ukraine, Timiryazevskaya Str. 2, 252014, Kiev, Ukraine*

Received 20 September 1997; in revised form 11 August 1998

Abstract

Center-cracked panels loaded in biaxial tension are examined in this paper. Calibration relations for the J integral and the Q constraint factor are presented for a Ramberg–Osgood power law hardening material under plane stress and plane strain loadings. Two cases are examined: an isolated crack and a periodic array of cracks both under biaxial loading conditions. The latter has previously been studied for plane stress conditions. A number of different J estimation schemes are proposed based on the remote load and displacement and their dependence on geometry, biaxiality, and material properties is discussed. The variation of constraint, as characterised by Q, is also presented for plane stress and plane strain conditions. Simple slip line field solutions are derived for perfectly plastic conditions and the resulting limit load solutions are compared with numerically determined values. Implications for failure of cracked plates under biaxial loading are discussed.

1. Introduction

With the increased interest in the effect of 'state of stress' or constraint on fracture toughness, there has been a corresponding increase in interest in biaxial testing. By varying the magnitude of the load applied parallel to the crack (See Fig. 1) different levels of constraint can be generated. The behaviour of biaxially loaded panels has been examined in Lee and Liebowitz (1977) where elastic-plastic calculations were carried out to explain the dependency of fracture toughness on biaxiality observed in Kibler and Roberts (1970). In Jansson (1986), J solutions for a periodic array of cracks under plane stress conditions were obtained and in Dowling (1987) J solutions for

* Corresponding author. Tel.: 0044 171 594 7059; fax: 0044 171 823 8845; e-mail: n.odowd@ic.ac.uk

0020-7683/99/$ - see front matter
PII: S0020-7683(98)00257-1

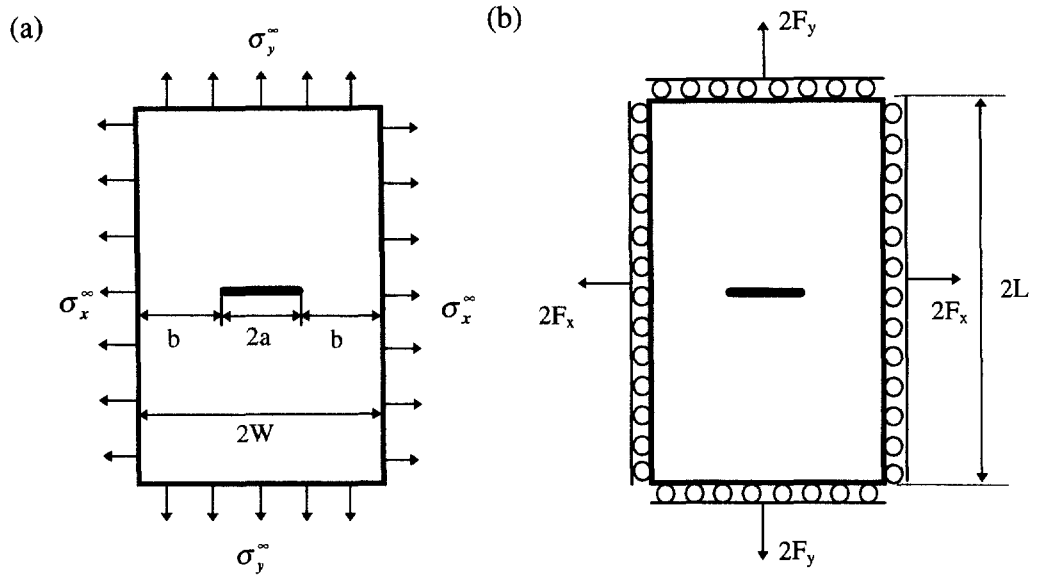

Fig. 1. Geometries examined, (a) isolated crack (configuration A) and (b) periodic array of cracks (configuration B).

biaxially loaded cracks in infinite bodies were presented. More recently, the effect of biaxiality on fracture toughness has been examined in Chao and Lam (1996), Wright et al. (1994) and Pennell et al. (1994). However, despite the large amount of research in the area of biaxial loading, solutions for J and the constraint parameter Q, (O'Dowd and Shih 1991), for biaxially loaded plates are rather limited. As discussed later, the elastic T stress also used to characterise state of stress effects (Betegón and Hancock, 1991), may be obtained simply by adding the magnitude of the horizontal stress to the T stress value for a uniaxially loaded plate.

In this paper, J and Q solutions determined by finite element analysis are presented. Results are presented for plane stress and plane strain conditions and for two types of biaxial loading. The two geometries are illustrated in Fig. 1. The first case, henceforth designated configuration A, is an isolated crack subjected to remote biaxial stress σ_x^∞ and σ_y^∞ and the second case, designated configuration B, has the remote boundaries held straight, but free to slide in the tangential direction. The latter loading condition, corresponds to an infinite periodic array of cracks and has been used in Jansson (1986) to approximate the loading condition of a cruciform specimen with a thinner center-section. The biaxiality is defined by the ratio, $B = \sigma_x^\infty/\sigma_y^\infty$, which is equal to F_x/F_y when the height of the specimen $2L$ is equal to the width $2W$.

2. Material properties and finite element model

The material is characterised by a Ramberg Osgood power law hardening model. Under uniaxial tension this is represented by

$$\varepsilon/\varepsilon_0 = \sigma/\sigma_0 + \alpha(\sigma/\sigma_0)^n \tag{1}$$

This material law is in effect a non-linear elastic law and can be applied to a power law plastic material (flow theory material) under conditions of proportional loading. In this work, the value of α was taken to be 1, the Young's modulus ($E = \sigma_0/\varepsilon_0$) and was 500 σ_0 and Poisson's ratio was 0.3.

A focused finite element mesh, with four noded quadrilaterals similar to that used in O'Dowd and Shih (1991) is employed. A typical mesh contains 1500 nodes and 1200 elements; the smallest element used was 1/1000 of the crack length. The crack length to specimen width, a/W, ratio ranges from 0.1 to 0.5. The majority of the data presented is for a specimen height to width, L/W, ratio of 2. As will be seen, for $L/W \geqslant 2$, the J normalisations are independent of L/W. The specimens are loaded proportionally with $\sigma_x^{\infty} = \mathrm{B}_y^{\infty}$ for configuration A and $F_x = (LB/W)F_y$ for configuration B. The finite element program ABAQUS (1996) has been used to obtain the solution to this boundary value program. Results for the normalising parameters will be presented under conditions of large scale plasticity when the plastic strains dominate and the material behaviour is very close to pure power law behaviour. Under these conditions the standard EPRI approach for pure power law materials (Kumar et al., 1981) is relevant and the η value (Turner, 1973) is independent of load.

3. *J* Normalisations

Biaxial loading of a periodic array of cracks (configuration B) was studied in Jansson (1986) under conditions of plane stress. A normalisation of the following form was employed:

$$J = a\gamma\sigma_0\varepsilon_0(1-a/W)f_1(n, a/W, B)\left(\frac{\sigma_{en}}{\sigma_0}\right)^{n-1}\left(\frac{\sigma_{yn}}{\sigma_0}\right)^2 \tag{2}$$

where $\gamma = 1$ and σ_{yn} is the nominal remote stress normal to the crack,

$$\sigma_{yn} = \frac{F_y}{t(W-a)} \tag{3}$$

where t is specimen thickness and σ_{en} is the nominal von Mises stress, defined in plane stress as

$$\sigma_{en}^2 = \sigma_{yn}^2 + \sigma_{xn}^2 - \sigma_{yn}\sigma_{xn} \tag{4}$$

with σ_{xn} the nominal remote stress parallel to the crack,

$$\sigma_{xn} = \frac{F_x}{tL} \tag{5}$$

In the current work, plane strain conditions are also examined and the nominal von Mises stress is given by

$$2\sigma_{en}^2 = (\sigma_{xn}-\sigma_{yn})^2 + (\sigma_{yn}-\sigma_{zn})^2 + (\sigma_{xn}-\sigma_{zn})^2 \tag{6}$$

with

$$\sigma_{zn} = 0.5(\sigma_{xn}+\sigma_{yn}) \tag{7}$$

and γ in eqn. (2) is 3/4. The above normalisation has the property that it reduces to the standard EPRI scheme of Kumar et al. (1981) for uniaxial loading and that the function f_1 is independent of biaxiality for $n = 1$, i.e. the stress parallel to the crack does not effect K or J for linear elastic conditions. While this normalization works well for plane stress conditions, it will be seen that it results in very large values of f_1 for high biaxiality ratios in plane strain. For this reason a second normalisation is investigated which is closer in form to the EPRI solutions,

$$J = a\varepsilon_0\sigma_0(1-a/W)h_1(n, a/W, B)(F_y/F_{yo})^{n+1} \tag{8}$$

where F_{yo} is the appropriate limit load which will be determined numerically (a brief discussion of limit load behaviour follows in Section 4). In this case, h_1 will not be independent of biaxiality for $n = 1$ as the limit load will depend on B.

Two other normalisations for J were examined which used modified versions of the standard η approach (e.g. Turner, 1973; Rice et al., 1973) for J evaluation,

$$J = \frac{\eta_1}{(W-a)t}\text{work done} = \frac{\eta_1}{(\mathrm{W}-\mathrm{a})\mathrm{t}}\left(\int \mathrm{F}_y\,\mathrm{d}\,\Delta_y + \int F_x\,\mathrm{d}\,\Delta_x\right) \tag{9}$$

With Δ_y and Δ_x the average remote displacements corresponding to F_y and F_x respectively. Since the loading is proportional, F_x/F_y is constant, the two terms in the above equation are not independent. It may prove simpler to combine F_y and F_x to write

$$J = \frac{\eta_2}{(W-a)t}\int F_y\,\mathrm{d}\,\Delta_y \tag{10}$$

This allows calculation of J from a record of a single load displacement history. Of course in general η_1 and η_2 from eqns (9) and (10) will differ.

4. Estimates of limit load

The limit load is used in the normalisation for J proposed in the previous section. Numerical solutions for the limit load will be used in the paper, but it also proves useful to derive approximate limit load solutions.

For a center-cracked panel under uniaxial loading, the values of the stresses ahead of the crack may be determined from the plane strain slip line fields, giving

$$\sigma_y = 2\sigma_0/\sqrt{3};\quad \sigma_x = 0;\quad \sigma_{xy} = 0 \tag{11}$$

where σ_0 is the von Mises yield stress. For biaxial loading, $\sigma_x^\infty = \mathrm{B}\sigma_y^\infty$ we can add a hydrostatic stress to the stress field in the forward sector, $-\pi/4 < \theta < \pi/4$, giving,

$$\sigma_y = 2\sigma_0/\sqrt{3} + B\sigma_y^\infty;\quad \sigma_x = B\sigma_y^\infty;\quad \sigma_{xy} = 0 \tag{12}$$

Note that a hydrostatic stress does not effect yield so the yield criterion is unaffected. By applying global equilibrium to the above field, we obtain

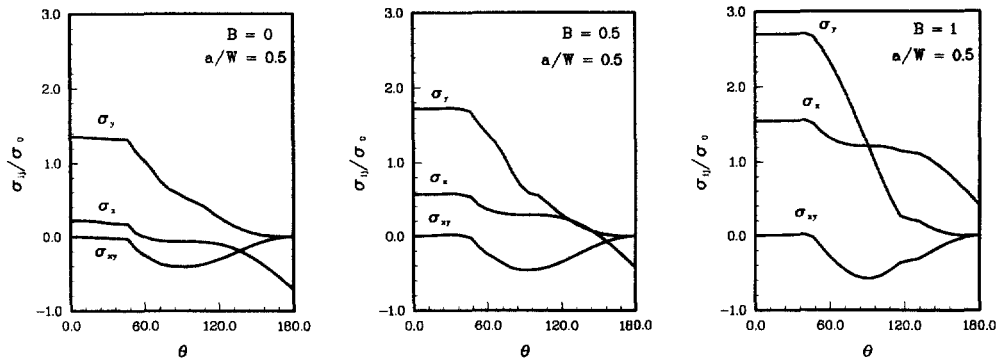

Fig. 2. Near tip finite element stress fields for perfectly plastic material.

$$\sigma_y = \frac{2\sigma_0}{\sqrt{3}}\left(\frac{1}{1-(1-a/W)B}\right)$$
$$\sigma_x = \frac{2\sigma_0}{\sqrt{3}}\left(\frac{B(1-a/W)}{1-B(1-a/W)}\right) \tag{13}$$

The stress fields for three biaxialities, $B = 0$, 0.5 and 1.0, determined from a finite element analysis of an elastic perfectly plastic material, are shown in Fig. 2 or $a/W = 0.5$. Here the angular variation of the stresses close to the crack tip is plotted. The stresses vary somewhat with distance from the crack tip and have been plotted at $r/a = 0.05$. The increase in near tip constraint (i.e. the values of σ_x and σ_y) with B is evident. Note that for $B = 1$ the stress fields approach the Prandtl stress field which is considered to be the limiting distribution for a crack in a rigid perfectly plastic material (Hutchinson, 1968). It may be seen that, though not identical, the stress in the forward sector, $-\pi/4 < 0 < \pi/4$, are well represented by eqn (13).

If it is assumed that the stress fields of eqn (13) extend over the uncracked ligament, the limit load, F_{y0} may be determined as

$$F_{y0} = \frac{2\sigma_0}{\sqrt{3}}\frac{(W-a)t}{1-B(1-a/W)} \tag{14}$$

Equation 14 reduces to the well known limit load expression for a uniaxially loaded panel when $B = 0$. Note the strong dependence of the limit load on B and for $a/W \to 0$, $B = 1$, $F_{y0} \to \infty$.

The ratio between the numerically determined limit load and the estimate given by eqn (14) is plotted in Fig. 3(a) for a range of cases. It may be seen that apart from the $B = 1$ case for $a/W < 0.5$ the numerical limit load is close to the value given by eqn (14). The reason for the poor agreement for the case of $B = 1$ is illustrated in Fig. 4. Here the zone of intense plastic strain determined from the finite element analysis is shown for a number of cases (highest plastic strains are in red). For the case of $B = 1$, $a/W = 0.1$ and 0.25, it may be seen that the plastic zone does not extend across the ligament, but instead surrounds the crack tip. Hence the assumption on which eqn (14) is based is invalid and the limit load is considerably overestimated. It is clear therefore that eqn (14) is not a lower bound limit load solution, despite the fact that a solution apparently satisfying yield

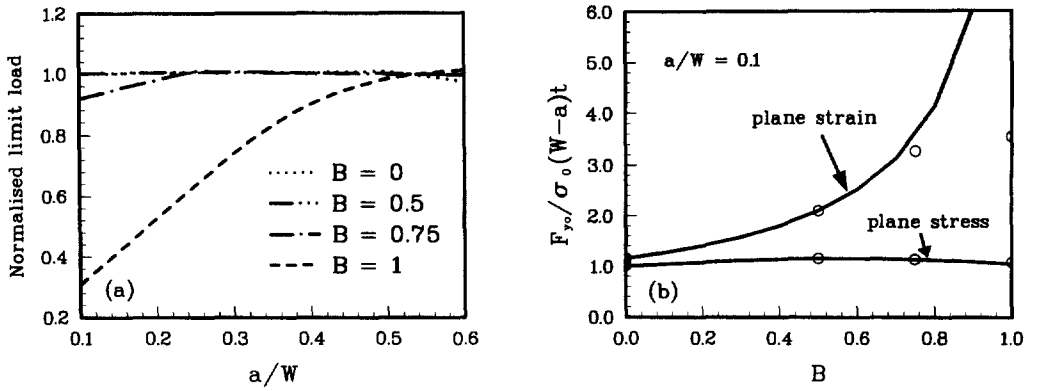

Fig. 3. (a) Numerical limit load normalised by approximate limit load solution, eqn (14). (b) Normalised value of plane strain and plane stress limit load, F_{y0}. Finite element results indicated by the symbols.

has been obtained. However, it should be pointed out that equilibrium is not guaranteed to be satisfied in the back sector, $\pi/2 < \theta < -\pi/2$, since for a stress free crack face, $\sigma_y = 0$ and, for continuity of stress, $\sigma_x = B\sigma_y^{\infty}$. It may be shown that with these stresses, the yield criterion in the area above and below the crack will be satisfied and a lower bound limit load obtained if $B(2-a/W) \leqslant 1$. For $a/W = 0.5$ this requires $B \leqslant 0.66$ and for $a/W = 0.1$, $B \leqslant 0.53$ which is consistent with the results shown in Fig. 3(a).

For the case of plane stress, the near tip fields may be determined assuming that $\sigma_x = B\sigma_y^{\infty}$ and invoking the von Mises yield condition and global equilibrium. We then obtain

$$\sigma_y = \frac{\sigma_0}{\sqrt{1-B(1-a/W)+B^2(1-a/W)^2}}$$
$$\sigma_x = \frac{B\sigma_0}{\sqrt{1-B(1-a/W)+B^2(1-a/W)^2}} \tag{15}$$

The limit load obtained from this stress field is then,

$$F_{y0} = \frac{\sigma_0(W-a)t}{\sqrt{1-B(1-a/W)+B^2(1-a/W)^2}} \tag{16}$$

The above limit load solution has also been proposed in Dalle Donne and D'Oker (1994).

Our finite element solutions are closely in agreement with eqn (16) for all the cases examined. This is illustrated in Fig. 3(b) for $a/W = 0.1$. The plane strain result, eqn (14), is also shown. Here the symbols are the FE solutions and the solid lines represent eqns (14) and (16). Note that, in contrast to the plane strain result, eqn (16) predicts a weak dependence of the limit load on B. For $B = 1$, $a/W \to 0$, $F_{y0} \to \sigma_0 (W-a)$ the same result as for $B = 0$. In the sections which follow the numerically determined limit load is used as the normalising load and the same limit loads have been used for configurations A and B, though in practise they will differ from one another. For example for $B = 1$, $a/W = 0.1$ the limit load for configuration B under plane strain is 5% higher than for configuration A.

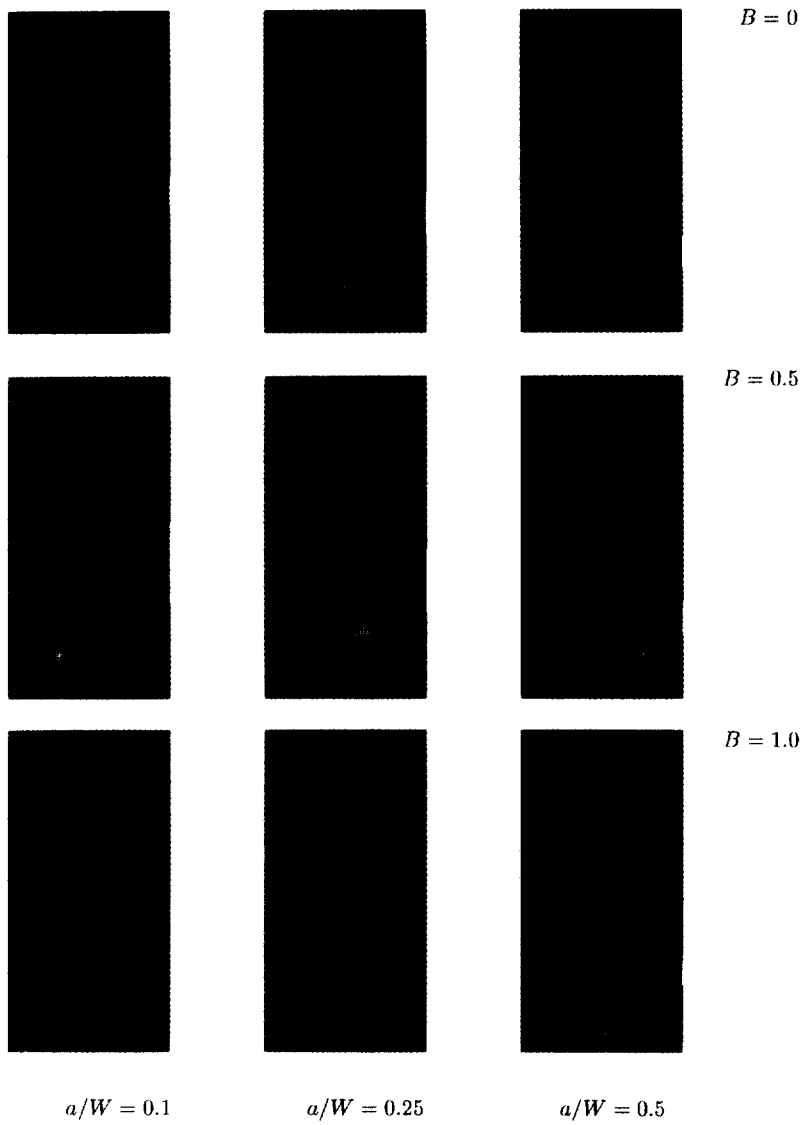

Fig. 4. Plastic zones in biaxially loaded panels, determined from finite element analysis, for a perfectly plastic material.

5. Results of J normalisations

The results of the different normalisations are given in Tables 1–6 for a range of a/W ratios, hardening exponents and biaxiality ratios. In Fig. 5 the values of h_1 for $B = 0$ are plotted under plane strain and plane stress conditions. For each configuration, solutions were obtained for $n = 1$, 5, 10 and 20. (Note that $h_1 = f_1$ when $B = 0$.) Figure 5(a) and (b) correspond to configuration A, remote boundaries free and Fig. 5(c) and (d) correspond to Configuration B, remote boundaries straight.

There are some differences (maximum of about 20%) between the results in Fig. 5(a) and (b) and the EPRI solution particularly for high n values and deep cracks, $a/W = 0.5$. Similar differences have been reported in Lei and Ainsworth (1997) and Lee and Bloom (1993) for a number of geometries at large n values. In Fig. 5(d) the normalisation in Jansson (1986) is included for comparison. The close correspondence may be seen. It should be pointed out, however, that in this case there are also some differences between the present results and those in Jansson (1986). This is due to the different L/W ratios employed. It is stated in Jansson (1986) that the J normalisation is independent of L/W when $L/W \geqslant 1$. However, our results suggest that this is not in fact the case. In Fig. 6 h_1 is plotted against L/W for $n = 10$ and 20, $a/W = 0.5$. Here the value of h_1 normalised by the value at $L/W = 3$ is plotted for $1 < L/W < 3$. It is seen that the solution does not converge to a constant value until $L/W \geqslant 2$. The solutions obtained from our analysis for $L/W = 1$ agree with those in Jansson (1986) to within 2%.

In Figs 7 and 8, the f_1 function defined in eqn (2) is plotted for the four configurations with $B = 0.5$ and 1 respectively. Again the good agreement with the trend of the Janssen result may be

Table 1
J normalisation functions for $n = 4$, Configuration A

		Plane strain				Plane stress			
B	a/W	h_1	f_1	η_1	η_2	h_1	f_1	η_1	η_2
0	0.1	4.84	4.84	0.198	0.198	4.69	4.69	0.193	0.193
0	0.25	3.48	3.48	0.479	0.479	3.24	3.24	0.453	0.453
0	0.5	2.13	2.13	0.715	0.715	1.95	1.95	0.695	0.695
0.5	0.1	14.2	4.29	0.810	0.425	5.70	4.29	0.234	0.234
0.5	0.25	6.96	2.72	1.38	0.830	3.67	2.81	0.515	0.507
0.5	0.5	2.98	1.68	1.18	0.875	2.09	1.70	0.775	0.737
0.75	0.1	27.3	4.38	2.72	0.999	4.97	3.88	0.185	0.239
0.75	0.25	12.5	2.40	2.05	1.10	3.50	2.64	0.414	0.507
0.75	0.5	3.68	1.44	1.50	0.952	2.12	1.62	0.695	0.734
1.0	0.1	12.7	80.7	5.82	12.2	4.02	3.66	0.132	0.260
1.0	0.25	8.50	5.77	2.17	3.93	3.32	2.70	0.304	0.547
1.0	0.5	5.10	1.28	1.64	1.13	3.24	2.63	0.296	0.533

Table 2
J normalisation functions for $n = 10$, Configuration A

		Plane strain				Plane stress			
B	a/W	h_1	f_1	η_1	η_2	h_1	f_1	η_1	η_2
0	0.1	5.70	5.70	0.342	0.342	5.66	5.66	0.339	0.339
0	0.25	3.19	3.19	0.804	0.804	2.98	2.98	0.777	0.777
0	0.5	1.63	1.63	0.903	0.903	1.52	1.52	0.902	0.902
0.5	0.1	14.4	4.37	1.38	0.739	6.37	4.79	0.377	0.374
0.5	0.25	5.51	2.15	1.54	0.967	3.11	2.38	0.826	0.787
0.5	0.5	2.23	1.26	1.27	0.953	1.60	1.30	0.986	0.915
0.75	0.1	20.3	5.39	2.85	1.31	5.15	4.02	0.257	0.326
0.75	0.25	8.38	1.60	2.14	1.03	2.78	2.10	0.641	0.721
0.75	0.5	2.73	1.07	1.56	0.977	1.57	1.20	0.961	0.910
1.0	0.1	5.51	10^5	4.12	7.78	3.92	3.57	0.153	0.296
1.0	0.25	5.05	60.0	1.61	2.82	2.41	1.96	0.395	0.644
1.0	0.5	3.51	0.877	1.92	1.01	1.48	1.11	0.857	0.893

Table 3
J normalisation functions for $n = 20$, Configuration A

		Plane strain				Plane stress			
B	a/W	h_1	f_1	η_1	η_2	h_1	f_1	η_1	η_2
0	0.1	5.52	5.52	0.603	0.603	5.60	5.60	0.605	0.605
0	0.25	2.49	2.49	0.946	0.946	2.43	2.43	0.944	0.944
0	0.5	1.25	1.25	0.965	0.965	1.22	1.22	0.965	0.965
0.5	0.1	11.9	3.59	1.66	0.924	5.97	4.49	0.625	0.613
0.5	0.25	4.12	1.61	1.58	0.989	2.60	1.99	1.01	0.949
0.5	0.5	1.69	0.953	1.31	0.983	1.33	1.08	1.04	0.966
0.75	0.1	15.6	9.60	2.67	1.38	4.24	3.31	0.388	0.480
0.75	0.25	6.13	1.17	2.22	1.02	2.16	1.63	0.938	0.974
0.75	0.5	2.06	0.803	1.60	0.998	1.30	0.996	1.03	0.965
1.0	0.1	1.58	10^8	3.55	6.31	3.04	2.76	0.182	0.347
1.0	0.25	2.81	10^5	1.43	2.45	1.52	1.24	0.575	0.816
1.0	0.5	2.60	0.650	2.01	1.00	1.17	0.874	0.975	0.960

seen for the plane stress case. As may be seen from Tables 2 and 3, the plane strain f_1 values are very large for $B = 1$ and large values of n and therefore are not plotted. It is clear that the nominal effective stress underestimates the influence of the load in this case. The use of the limit load as

Table 4
J normalisation functions for $n = 4$, Configuration B

		Plane strain				Plane stress			
B	a/W	h_1	f_1	η_1	η_2	h_1	f_1	η_1	η_2
0	0.1	4.38	4.38	0.180	0.180	4.33	4.33	0.179	0.179
0	0.25	2.35	2.35	0.342	0.342	2.45	2.45	0.357	0.357
0	0.5	0.811	0.811	0.423	0.423	1.16	1.16	0.542	0.542
0.5	0.1	11.3	3.42	0.665	0.344	5.52	4.16	0.227	0.227
0.5	0.25	3.75	1.46	0.958	0.550	3.33	2.55	0.475	0.471
0.5	0.5	0.893	0.502	0.861	0.597	1.69	1.38	0.696	0.687
1.0	0.1	12.6	79.9	4.96	6.85	4.02	3.65	0.132	0.260
1.0	0.25	8.38	5.69	2.26	2.56	3.20	2.60	0.293	0.528
1.0	0.5	3.22	0.804	1.22	1.23	2.03	1.52	0.525	0.716

Table 5
J normalisation functions for $n = 10$, Configuration B

		Plane strain				Plane stress			
B	a/W	h_1	f_1	η_1	η_2	h_1	f_1	η_1	η_2
0	0.1	3.88	3.88	0.240	0.240	3.90	3.90	0.241	0.241
0	0.25	0.935	0.935	0.400	0.400	1.07	1.07	0.446	0.446
0	0.5	0.0693	0.0693	0.421	0.421	0.314	0.314	0.791	0.791
0.5	0.1	6.75	2.04	0.817	0.426	5.83	4.38	0.348	0.347
0.5	0.25	0.852	0.333	0.950	0.564	2.51	1.92	0.748	0.742
0.5	0.5	0.0399	0.0224	0.801	0.554	0.917	0.745	0.899	0.898
1.0	0.1	4.53	10^5	3.86	3.90	3.89	3.54	0.151	0.294
1.0	0.25	4.32	51.3	1.70	1.74	2.31	1.88	0.384	0.627
1.0	0.5	0.666	0.166	1.09	1.10	1.42	1.06	0.846	0.888

Table 6
J normalisation functions for $n = 20$, Configuration B

		Plane strain				Plane stress			
B	a/W	h_1	f_1	η_1	η_2	h_1	f_1	η_1	η_2
0	0.1	2.30	2.30	0.312	0.312	2.18	2.18	0.297	0.297
0	0.25	0.172	0.172	0.429	0.429	0.214	0.214	0.522	0.522
0	0.5	10^{-3}	10^{-3}	0.431	0.431	0.055	0.055	1.00	1.00
0.5	0.1	2.62	0.793	0.888	0.486	5.18	3.90	0.571	0.568
0.5	0.25	0.0603	0.0236	0.923	0.525	1.79	1.37	0.937	0.936
0.5	0.5	10^{-4}	10^{-4}	0.775	0.533	0.480	0.390	0.959	0.959
1.0	0.1	1.18	10^6	3.48	3.48	2.88	2.62	0.173	0.331
1.0	0.25	2.00	10^4	1.50	1.50	1.23	0.996	0.529	0.755
1.0	0.5	0.050	0.0125	1.05	1.05	1.11	0.834	0.958	0.958

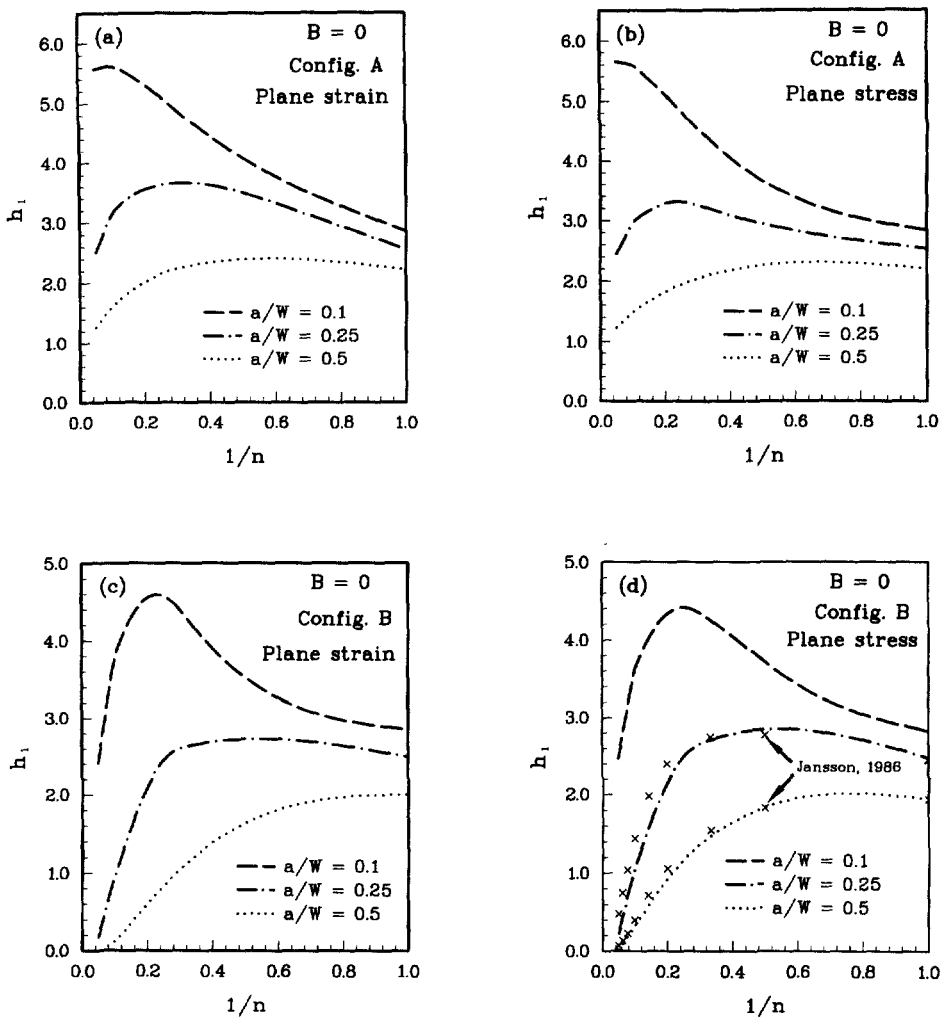

Fig. 5. Normalisation functions, h_1, for uniaxial loading, $B = 0$.

normalising load, i.e., using eqn (8) seems more appropriate in this case, though the values of h_1 obtained are still quite large (see Fig. 9).

The EPRI J estimation scheme described in Kumar et al. (1981) interpolates from the elastic region to the fully plastic regime. The value of J in the elastic-plastic regime is obtained by adding together the elastic J, J_e, determined from K and the plastic J, J_p, determined from one of eqns (2), (8), (9) or (10). A plastic zone correction may be applied to J_e to obtain an improved estimate for J as discussed in Kumar et al. (1981).

The results for the normalisation of eqns (9) and (10) are also shown in Tables 1–6. Again for $B = 0$ the normalisations are equivalent. The standard value for η for a uniaxially loaded center-cracked-tension geometry is 1 but it may be seen for a power law hardening material, η approaches unity only for shallow cracks and low hardening materials. Similar dependence of η on a/W and n

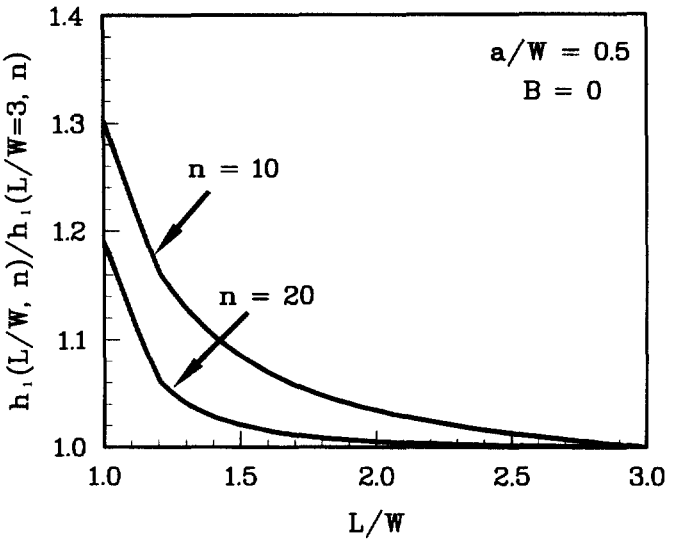

Fig. 6. Variation of normalisation function, h_1 with relative specimen height for $B = 0$, configuration A, plane strain.

have been reported in Kirk and Dodds (1991) for bend geometries. It may be seen in Tables 4–6 that for configuration B under plane stress conditions with biaxiality $B = 0.5$ the values of η_1 and η_2 are almost identical. This is because under these conditions the remote displacement parallel to the crack is negligible compared to the axial displacement. It may also be seen that in may cases η_1 is greater than η_2, this is due to the remote displacement parallel to the crack being negative even for biaxiality ratios as high as 0.75. This somewhat unexpected feature occurs mainly under plane strain conditions and arises due to the necessity to maintain incompressibility of plastic flow. The values of η_1 and η_2 become large for plane strain conditions and $B = 1$. However, the values obtained vary sensibly with geometry and loading and are considered to be a useful normalisation for this geometry.

6. Results of Q calculations

The Q parameter has been used to characterise constraint and size effects in crack geometries, e.g. O'Dowd and Shih (1991), where the near tip stresses are characterised by two parameters J and Q. It may be seen from the stress fields for a non-hardening material in Fig. 2 that the fields depend strongly on the biaxiality in the plane strain case and similar features are seen for the hardening material. The values of Q for $n = 10$ are shown in Figs 10 and 11 for the four configurations. Similar trends are seen for the other hardening exponents. In each case, Q is calculated by subtracting the numerically determined σ_y stress from the small scale yielding, $T = 0$ solution at $r/(J/\sigma_y) = 2$, $\theta = 0$ and dividing by the reference stress σ_y. Note that the small scale yielding distribution depends on whether conditions are plane stress or plane strain. Further details of the definition of the Q parameter are provided in O'Dowd and Shih (1991) and O'Dowd (1995). The

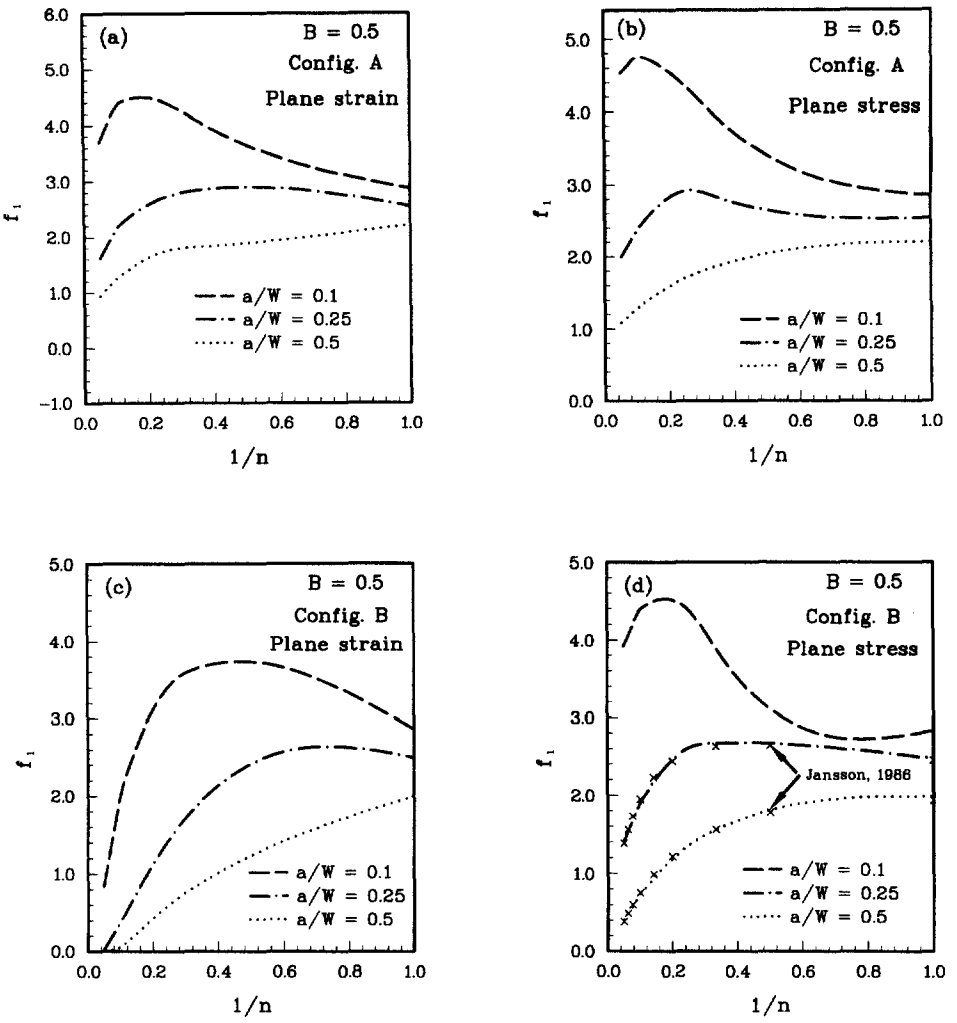

Fig. 7. Normalisation functions, f_1, for $B = 0.5$.

effect of load biaxiality on constraint in terms of the A_2 parameter has also been examined in Chao and Ji (1995).

For the case of $B = 0$ it is seen that in the plane strain case the constraint drops rapidly with increase in load. This well known feature has been presented elsewhere (O'Dowd and Shih, 1991; Chao and Ji, 1995; Betegón and Hancock, 1991). The same effect is seen for the collinear array of cracks, Fig. 10(d), although the loss of constraint is somewhat less in the latter case. Indeed for all biaxiality levels the collinear array gives a higher Q value than the isolated crack. Results are presented in Fig. 11, for plane stress with $B = 0$ and $B = 0.5$. The Q values for $B = 1$ are almost identical to those of $B = 0.5$. It may be seen there is very little loss of constraint as we move to fully yielded conditions. The lowest Q value is -0.2 compared with -1.5 for plane strain at the same level of J. This result is not unexpected—it was shown in Chao (1993) that the plane stress

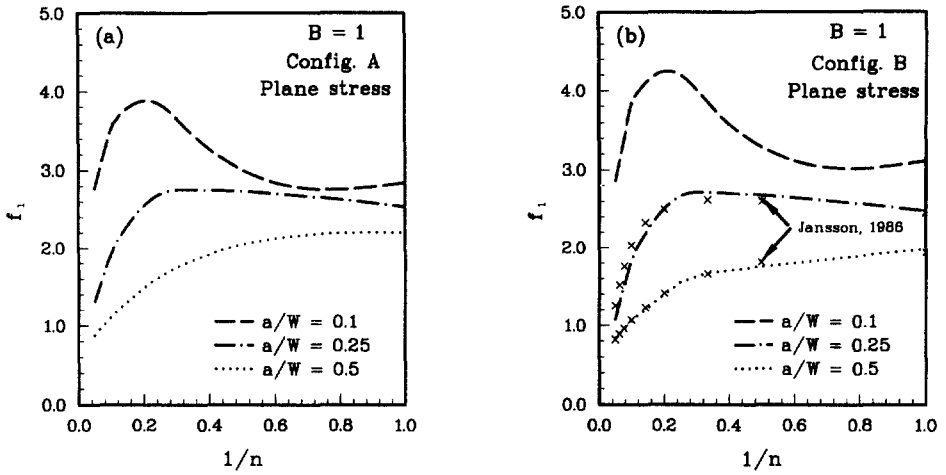

Fig. 8. Normalisation functions, f_1, for $B = 1$ for plane stress conditions.

crack tip fields are characterised by J for a range of constraint levels (controlled by the magnitude of the elastic T stress). The current analysis confirms that this feature carries over to finite geometries. A direct comparison between the plane stress and plane strain stress field cannot be made from Figs 10 and 11, since a different reference field has been used in each case to define Q. For $n = 10$, $\sigma_y^{ref}/\sigma_0 = 3.37$ in plane strain and $\sigma_y^{ref}/\sigma_0 = 1.75$ in plane stress. Examination of Figs 10 and 11 implies that at high loads, the plane stress distribution may approach the plane strain distribution.

7. Estimates of Q for plane strain using the elastic T stress

As discussed in Du and Hancock (1991) the elastic T stress provides a useful method of estimating constraint. The T stress is linearly proportional to the applied load, $T = \beta(a/W)\sigma_y^{\infty}$ and the function $\beta(a/W)$ has been tabulated for many geometries. Under plane strain conditions a one-to-one relationship for Q in terms of T is given in O'Dowd (1995) for $n = 10$.

$$Q = 0.8T/\sigma_0 - 0.5(T/\sigma_0)^2 \tag{17}$$

For a biaxially loaded specimen, with applied stress σ_x^{∞} parallel to the crack, by superposition, $T = T(\sigma_x^{\infty} = 0) + \sigma_x^{\infty}$. Specifically, for the case when $\sigma_x^{\infty} = B\sigma_y^{\infty}$ we get

$$T/\sigma_0 = (\sigma_y^{\infty}/\sigma_0)(\beta(a/W) + B) \tag{18}$$

This allows a direct estimate of Q to be made. In Fig. 12 the comparison is made for the three values of B examined under plane strain conditions and configuration A with $n = 10$. Similar behaviour has been seen for the other n values, ($n \geq 3$). It may be seen that in most cases the calculated Q value agrees well with the approximation from eqns (17) and (18). For the shallow crack, with $B = 0.5$, it is seen that Q first decreases and then increases. This behaviour was pointed

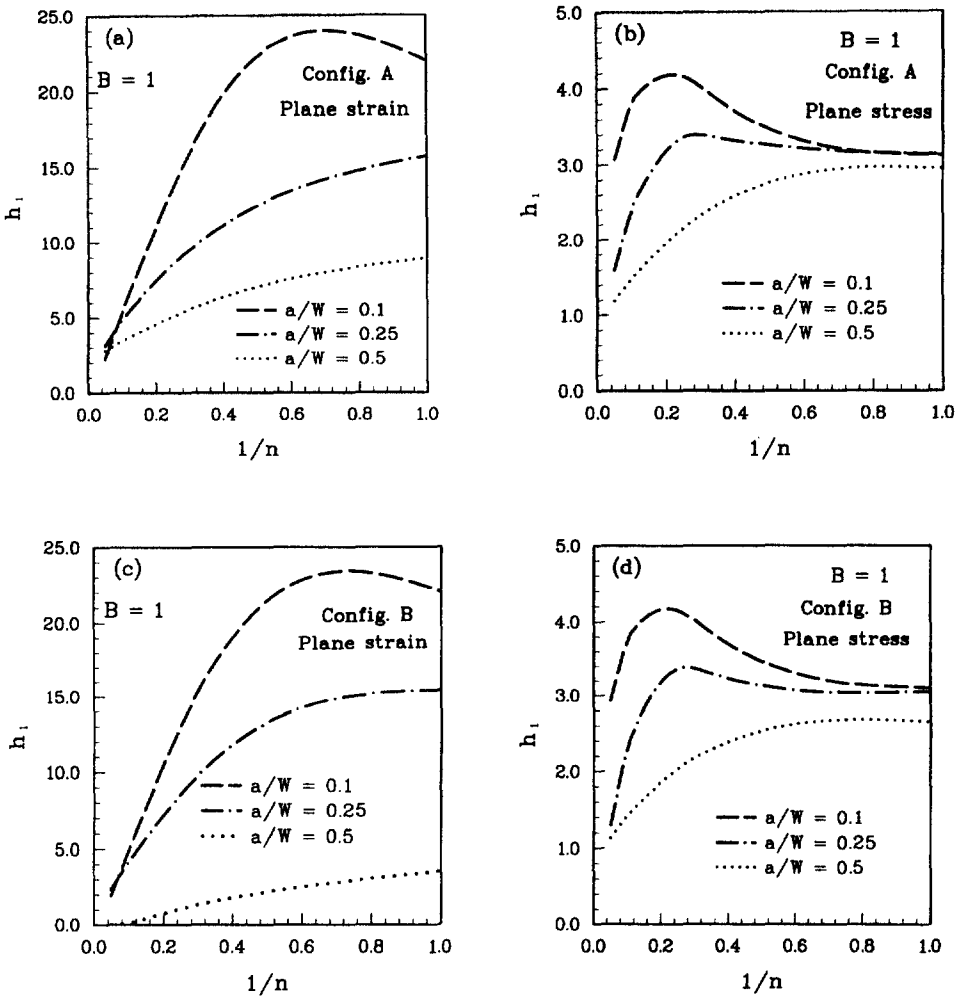

Fig. 9. Normalisation functions, h_1, for $B = 1$ for plane strain conditions.

out in O'Dowd and Shih (1991) and is somewhat surprising in view of the fact that the T stress decreases continuously. The reason for the observed behaviour may be seen by examining Fig. 13. The variation of Q with normalised distance for $B = 0.5$, $a/W = 0.1$ and 0.5, for load levels from contained yielding to fully yielded conditions is shown. The largest stress values in Fig. 13(a) and (b) correspond to 0.95 and 1.3 times the respective limit load. For $a/W = 0.1$, while Q is independent of distance from the crack tip at low load levels, at the highest load level there is a strong dependence on distance. In contrast the Q value for $a/W = 0.5$ remains sensibly independent of distance well into the fully plastic regime. The definition of Q and its relationship to the elastic T stress is closely tied to its independence of distance from the crack tip. Thus the definition of Q via the T stress will not work for this geometry. Indeed it is clear from Fig. 13(a) that if Q is evaluated at say $r = 0.2\ J/\sigma_0$ then it would be uniformly decreasing with increasing load. The reason that Q

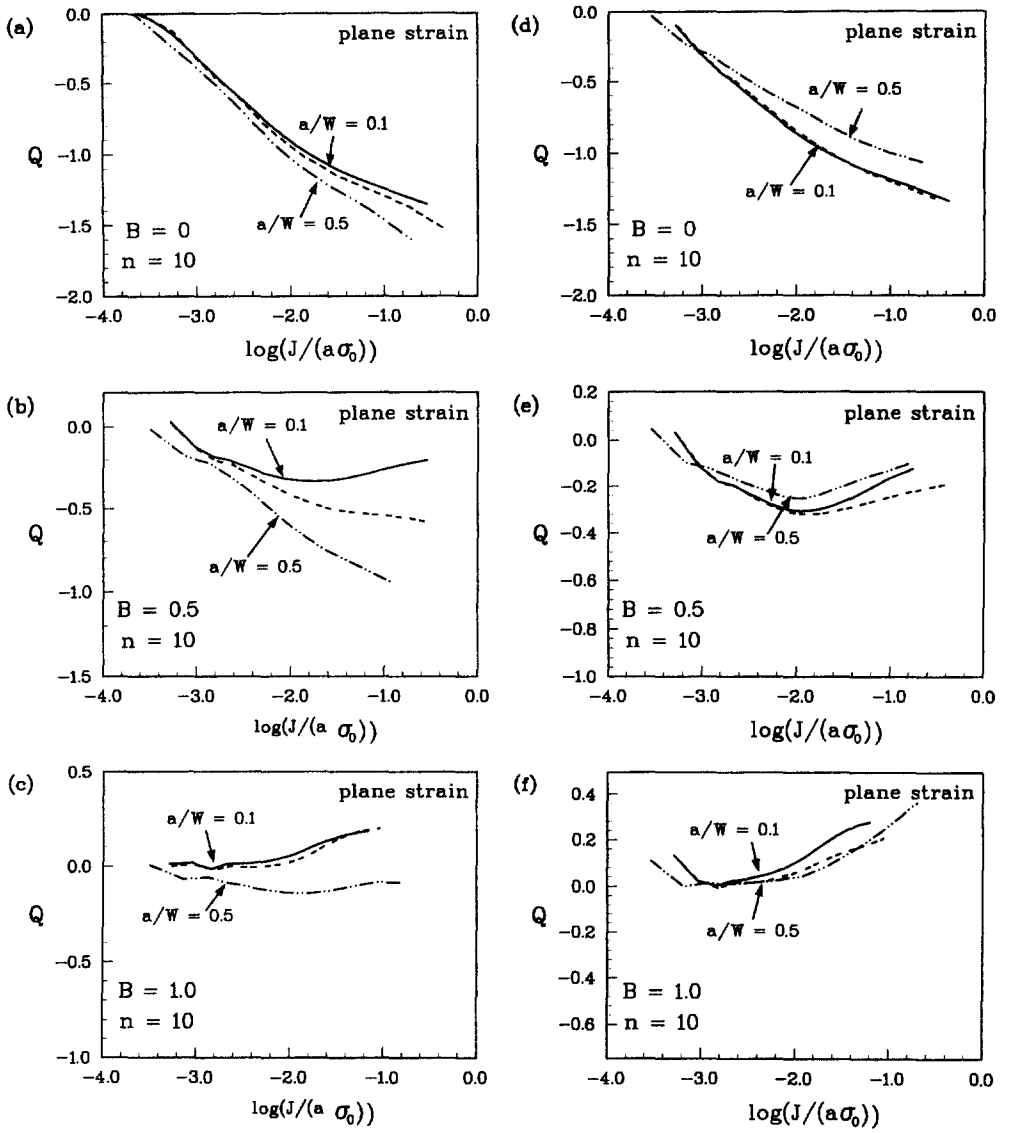

Fig. 10. Variation of Q with remote load for $n = 10$, plane strain conditions; (a)–(c) configuration A, (d)–(f) configuration B.

has been evaluated at $r = 2\ J/\sigma_0$ is because it is known that the crack tip opening displacement is of the order of J/σ_0. Therefore for distances less than J/σ_0 finite strain effects will dominate. In order for a solution based on small strain theory, as the J–Q theory is, to be useful it must dominate over regions greater than J/σ_0. It is still permissible to use the Q values in Fig. 13(a) at high load levels though whether this is an appropriate Q value will depend on what is the relevant physical distance for the material.

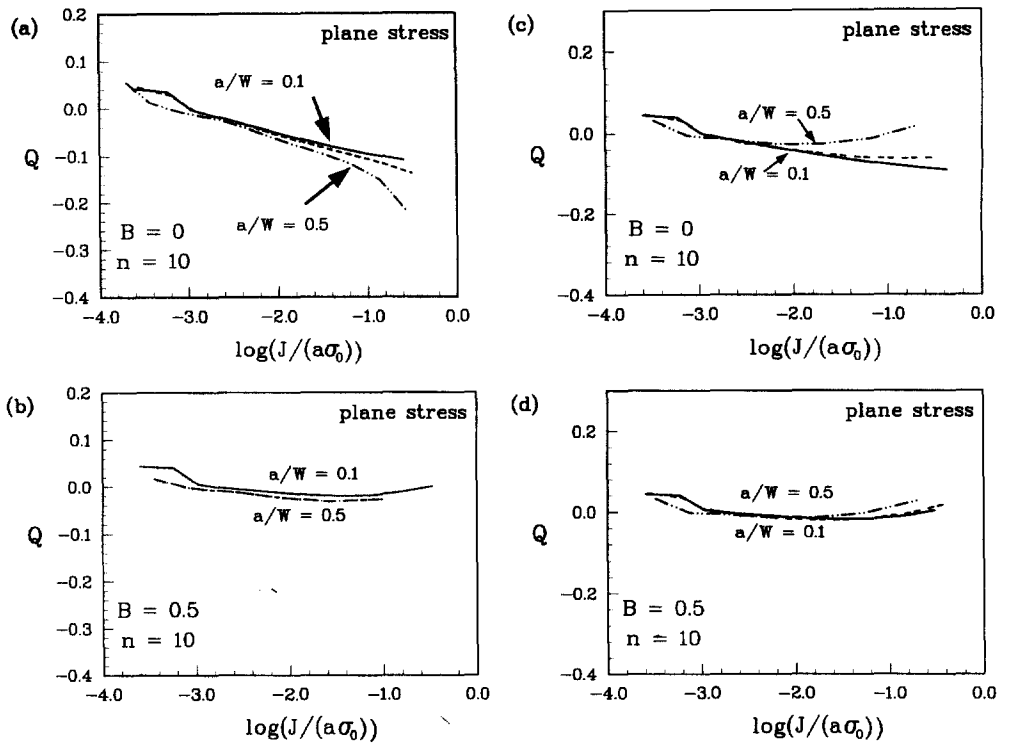

Fig. 11. Variation of Q with remote load for $n = 10$, plane stress conditions; (a), (b) configuration A, (c), (d) configuration B.

8. Effect of biaxiality on driving force for cleavage fracture

Under plane strain conditions increasing the biaxiality affects both J and Q—at the same level of remote load, σ_y^∞/σ_0, increasing B leads to an increase in Q and a decrease in the magnitude of J, (the latter is not immediately obvious from the normalisations used in the previous sections). Thus biaxial loading can lead to a decrease or an increase in the crack tip stresses and hence to an increase or decrease in the likelihood of cleavage fracture. This competing effect is illustrated in Fig. 14. It may be seen that at low load biaxiality B has little effect on J or Q, but as the load increases, increasing biaxiality leads to a dramatic decrease in J relative to the uniaxial case, Fig. 14(a) and an increase in Q, Fig. 14(b).

A direct comparison in terms of the near tip stress is next considered. Center cracked panels with $a/W = 0.5$ and $B = 0$ and 0.5 are examined. to quantify the combined effects of J and Q the stresses along the ligament are plotted at different remote stress levels for the two geometries in Fig. 15. Distances here are normalised by crack length a. At low loads the stress distributions are almost identical and correspond to the small scale yielding $T = 0$ solution. At intermediate loads $\sigma_y^\infty/\sigma_0 = 0.6$, the loss of constraint experienced by the uniaxially loaded specimen is the dominant effect and the distribution for the biaxially loaded specimen is above that of the uniaxially loaded

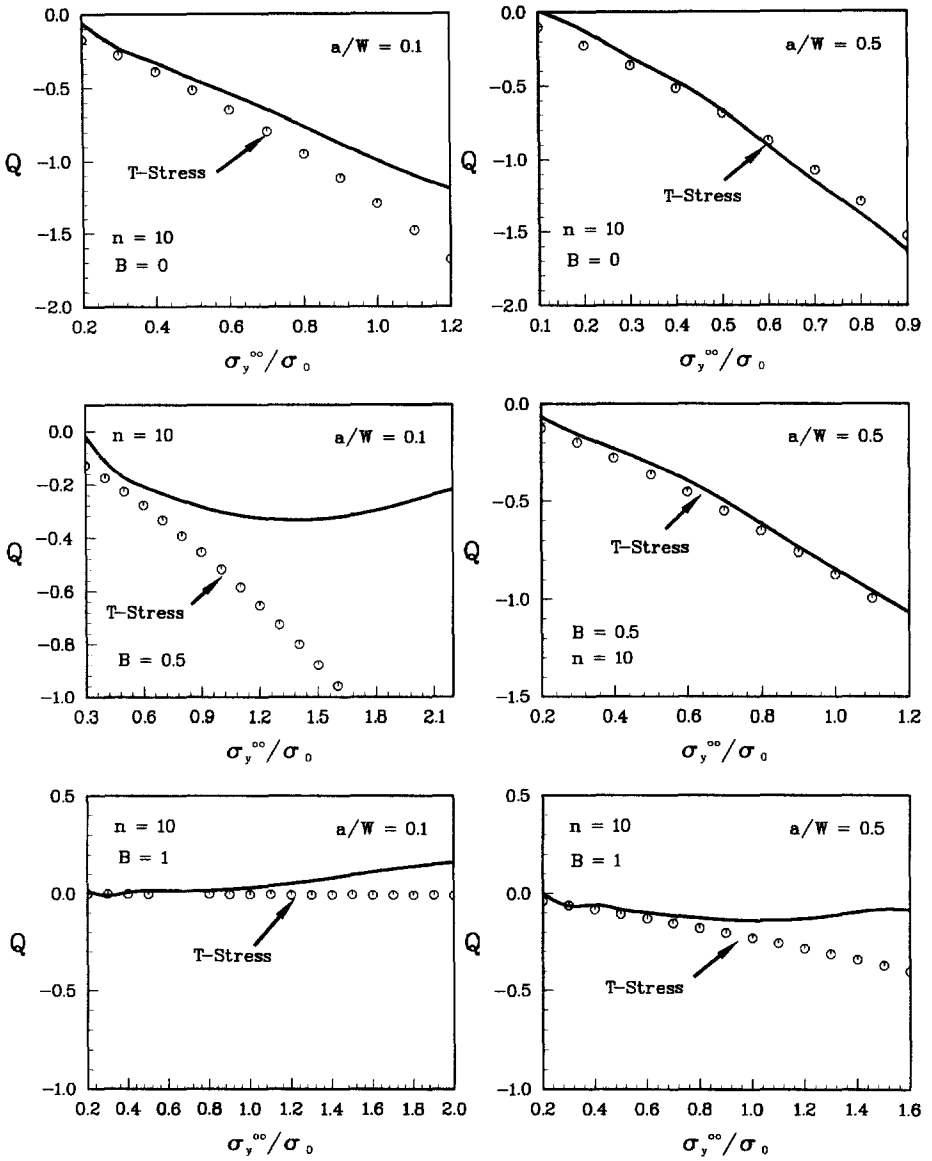

Fig. 12. Comparison between numerical Q values and T stress estimates for plane strain conditions, configuration A.

specimen. At even higher load $\sigma_y^\infty/\sigma_0 = 1.0$ the effect of J dominates so the uniaxial specimen experiences higher crack tip stresses than the biaxially loaded specimen.

An approach based on J_{Ic} would predict that the biaxially loaded specimen will always fail at a load equal to or above that of a uniaxially loaded specimen. However if the effect of constraint is included the absolute size of the specimens will determine which will fail first. In Fig. 16(a) and (b) a typical cleavage toughness $Jc(Q)$ locus (Sumpter and Forbes, 1992) is shown by the solid line. The equation for this curve is $J_c = J_{IC}(1-0.2Q)^6$. The J–Q load histories for $B = 0$ and

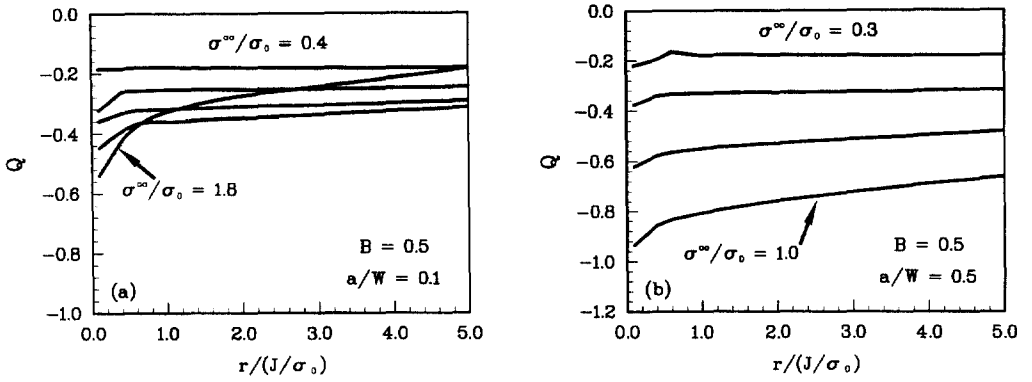

Fig. 13. Q plotted against normalised distance from the crack tip for $B = 0.5$, (a) $a/W = 0.1$, (b) $a/W = 0.5$.

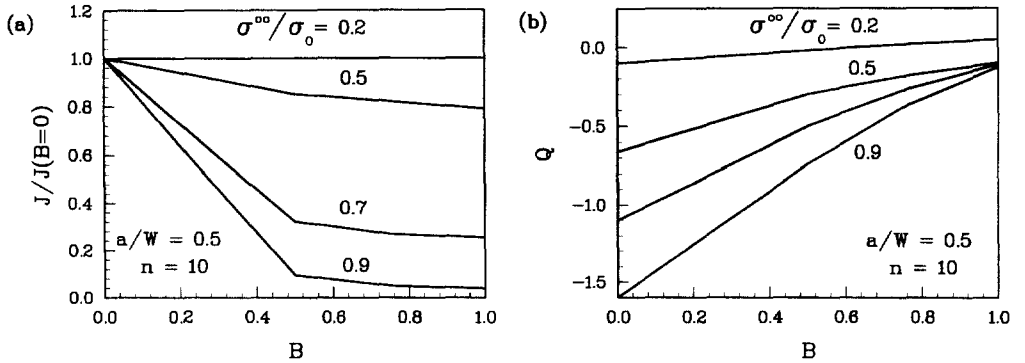

Fig. 14. Effect of biaxiality, B on (a) J and (b) Q at different load levels.

$B = 0.5$ are also shown with the corresponding load levels indicated at a number of points. Figure 16(a) considers a specimen where $a = 250\ J_{IC}\sigma_0$. In this case it is seen that the uniaxially loaded specimen will fail first at a load of about $\sigma^{\infty}_{yy}/\sigma_0 = 0.85$ while the biaxially loaded specimen will fail at $\sigma^{\infty}_{yy}/\sigma_0 \approx 0.9$. In contrast, Fig. 16(b) describes the behaviour for a larger specimen with $a = 1000\ J_{Ic}\sigma_0$, in this case both panels will fail at the same load of $\sigma^{\infty}_{yy}/\sigma_0 \approx 0.7$. Similar comparisons have been made in Chao and Ji (1995) where the A_2 constraint parameter has been used to compare the J value at cleavage for different crack geometries. An analysis has been carried out in Dodds et al. (1993) for surface cracks under biaxial and uniaxial loading. Their conclusions are consistent with those presented here—for large specimens biaxial loading is more severe due to the large decrease in constraint in the uniaxial specimen but for small specimens uniaxial loading is more severe due to the higher J value. Of course these predictions assume that the specimen fails by cleavage. It is possible that failure will initiate by ductile tearing at lower J values than would trigger cleavage. This issue is not examined in this paper.

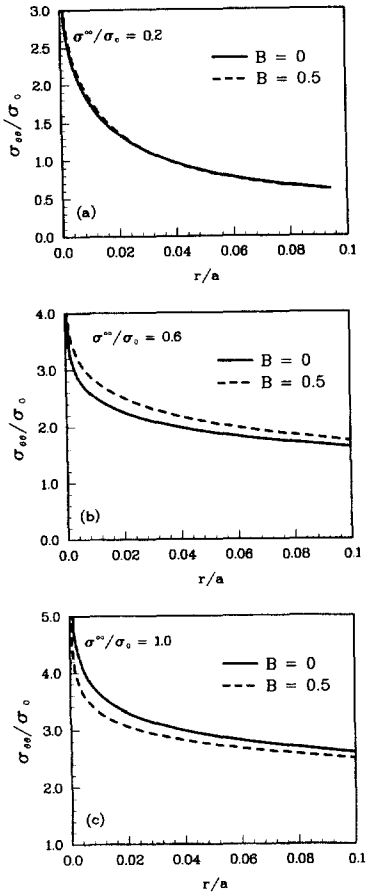

Fig. 15. Comparison between hoop stress ahead of a crack under uniaxial and biaxial loading for three load levels. Analysis is for plane strain, configuration A, $n = 10$, $a/W = 0.5$.

9. Concluding remarks

In this work biaxially loaded panels under plane stress and plane strain have been examined. A number of different normalisation functions are presented to allow calculation of J from experimental results. Solutions for the constraint parameter, Q, have also been presented and the ability of the T stress to predict Q under plane strain loading is examined. For the case of plane strain the limit load, J and Q values are all strongly dependent on biaxiality while for the case of plane stress all quantities depend weakly on biaxiality. The effect of biaxiality in reducing J but increasing Q has been discussed. Results have been presented for two different configurations, one where the boundaries of the plate are allowed to move freely and one where the boundaries are constrained. The decision as to which is more relevant will depend on the nature of the application of the loading.

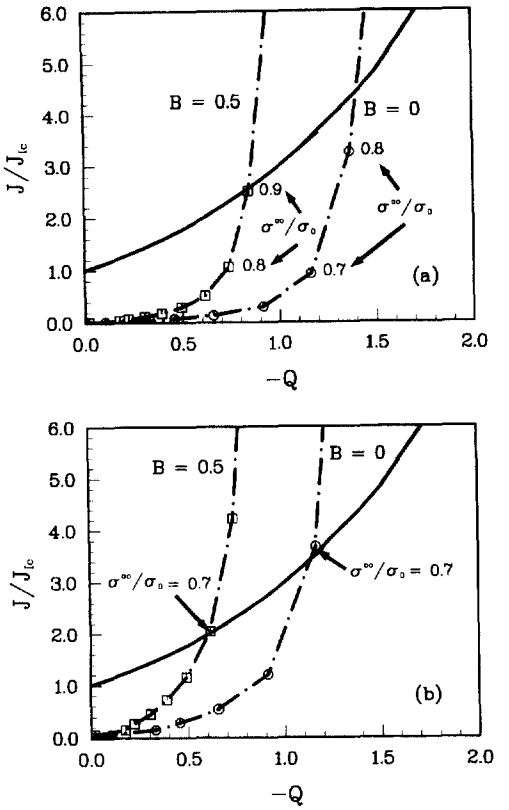

Fig. 16. Cleavage fracture behaviour for uniaxial and biaxial panels, (a) $a = 250\ J_{Ic}/\sigma_0$, (b) $a = 1000\ J_{Ic}$.

Acknowledgements

This study was partly funded by INTAS under the project number 94-722. The assistance of the Austrian Academy of Sciences with travel costs is also acknowledged. NPOD acknowledges helpful discussion with Dr JDG Sumpter of the DRA.

References

ABAQUS Version 5.5, 1996. Hibbit, Karlsson and Sorenson Inc., Providence, RI.

Betegón, C., Hancock, J.W., 1991. Two-parameter characterization of elastic-plastic crack-tip fields. J. Appl. Mech. 58, 104–110.

Chao, Y.J., 1993. On a single parameter controlled fracture of solids under plane stress conditions. Int. J. Frac. 62, R7–R10.

Chao, Y.J., Ji, W., 1995. Cleavage fracture quantified by J and A_2. In: Kirk M., Bakker, A. (Eds.), Constraint Effects in Fracture, Theory and Applications, ASTM STP 1244, pp. 3–20.

Chao, Y.J., Lam, P.S., 1996. Effects of crack depth, specimen size and out-of-plane stress on the fracture toughness of reactor vessel steels. J. of Press. Vess. Tech., Trans. ASME 118, 415–423.

Dalle Donne, C., Dóker, H., 1994. Biaxial load effects on plane stress $J-\Delta a$ and $\delta_5-\Delta a$ curves. In: Berger, C., Schwalbe,

K.H. (Eds.), Structural Integrity, Experiments—Models—Applications, Proceedings of ECF10, Vol. II, pp. 891–896.

Dodds, R.H., Shih, C.F., Anderson T.L., 1993. Continuum and micromechanics treatment of constraint in fracture. Int. J. Frac. 64, 101–133.

Dowling, N.E., 1987. *J* integral estimates for cracks in infinite bodies. Eng. Frac. Mech. 26, 333–348.

Du, Z.-Z., Hancock, J.W., 1991. The effect of non-singular stresses on crack-tip constraint. J. Mech. and Phys. Solids 39, 555–567.

Hutchinson, J.W., 1968. Singular behavior at the end of a tensile crack in a hardening material. J. Mech. Phys. Solids 16, 13–31.

Jansson, S., 1986. Fully plastic plane stress solutions for biaxially loaded centre-cracked plates. J. Appl. Mech. 53, 555–560.

Kibler, J.J., Roberts, R., 1970. The effect of biaxial stress on fatigue and fracture. J. Eng. Indust., Trans ASME 727–739.

Kirk, M.T., Dodds, R.H., 1991. Approximate techniques for predicting size effects on the cleavage fracture toughness (J_c). University of Illinois report, UILU ENG-91-2013.

Kumar, V., German, M.D., Shih, C.F. An engineering approach for elastic-plastic fracture analysis, EPRI Report NP-1931 (1981).

Lee, J.D., Liebowitz, H., 1977. Fracture criteria for crack growth under biaxial loading Eng. Fracture Mech. 9, 765–779.

Lee, D.R., Bloom, J.M., 1993. Assessment of fully plastic *J* and *C**-integral solutions for applications to elastic-plastic fracture and creep crack growth. J. Pres. Ves. Tech. Trans. ASME 15, 228–234.

Lei, Y., Ainsworth, R.A., 1997. The estimation of *J* in three point bend specimens with a crack in a mismatched weld. Int. J. Pres. Ves. and Piping 70, 247–257.

Naumenko, V.P., Kolednik, O., 1994. Load biaxiality effects on the fracture resistance of steel plates. In: Berger, C., Schwalbe, K.H. (Eds.), Structural Integrity, Experiments—Models—Applications, Proceedings of ECF10, Vol. II, 911–921.

O'Dowd, N.P., 1995. Applications of two parameter approaches in elastic-plastic fracture mechanics. Eng. Frac. Mech. 52, 45–465.

O'Dowd, N.P., Shih, C.F., 1991. Family of crack-tip fields characterized by a triaxiality parameter—I: structure of fields. J. Mech. Phys. Solids 39, 989–1015.

Pennell, W.E., Bass, B.R., Bryson, J.W., McAfee, W.J., Theiss, T.J., Rao, M.C., 1994. Biaxial loading and shallow-flaw effects on crack tip constraint and fracture toughness. Proceedings of the 1994 Pressure Vessels and Piping Conference. Minneapolis, MN, U.S.A., Jun 19–23, pp. 103–114.

Rice, J.R., 1968. A path independent integral and the approximate analysis of strain concentration by notches and cracks. J. Appl. Mech. 35, 379–386.

Rice, J.R., Paris, P., Merkle, J., 1973. Some further results of *J J*-integral analysis and estimates. Progress in Flaw Growth and Fracture Toughness Testing, ASTM STP 536, American Society for Testing and Materials, pp. 231–245.

Sumpter, J.D.G., Forbes, A.T., 1992. Constraint based analysis of shallow cracks in mild steel. Proceedings of TWI/E-WI/IS International Conference on Shallow Crack Fracture Mechanics Test and Applications, Cambridge, U.K.

Turner, C.E., 1973. Fracture toughness and specific fracture energy: a re-analysis of results. Mat. Sci. Engineering 11, 275–282.

Wright, D.J., Sharples, J.K., Sherry, A.H., Gardner, L., 1994. Effect of biaxial loading on the fracture behaviour of a ferritic steel component. Nuclear Eng. Design 152, 39–55.